Polymer 51 (2010) 3693–3705

Contents lists available at ScienceDirect

Polymer

journal homepage: www.elsevier.com/locate/polymer

Mesogen-jacketed liquid crystalline polymers substituted with oligo(oxyethylene) as peripheral chain

Xiaochao Liang [a], Xiaofang Chen [a], Christopher Y. Li [b,*], Zhihao Shen [a], Xinghe Fan [a], Qifeng Zhou [a,**]

[a] Beijing National Laboratory for Molecular Sciences, Key Laboratory of Polymer Chemistry and Physics of Ministry of Education, College of Chemistry and Molecular Engineering, Peking University, Beijing 100871, China
[b] Department of Materials Science and Engineering, Drexel University, Philadelphia, PA 19104, USA

ARTICLE INFO

Article history:
Received 26 March 2010
Received in revised form
19 May 2010
Accepted 21 May 2010
Available online 9 June 2010

Keywords:
Mesogen-jacketed liquid crystalline polymers
Liquid crystalline polymer
Oligo(oxyethylene)
Columnar nematic phase

ABSTRACT

Mesogen-jacketed liquid crystalline polymer (MJLCP) is a typical rod-shaped macromolecule. Its unique molecular architecture allows one to tune the geometric parameters of the macromolecular rod. Moreover, the rod surface chemistry can be controlled by designing the peripheral groups of the lateral mesogens. In previous work in this system, short alkyl chains have been used and the resultant macromolecular rods therefore have a hydrophobic surface. In this paper, we report using oligo(oxyethylene) groups as the peripheral groups of the lateral mesogens. Poly{{2,5-bis[4-methoxyoligo(oxyethylene)phenyl]oxycarbonyl}styene} (PnEOPCS) with different oligo(oxyethylene) chain length has been synthesized. These oligo(oxyethylene) groups led to macromolecular rods with hydrophilic surface. Differential scanning calorimetry, polarized light microscopy, and one-/two-dimensional wide-angle X-ray diffraction experiments were carried out to study the phase structures and phase behaviors of this series of polymer. The existence of flexible polar groups lowered the glass transition temperatures of PnEOPCS. All polymers studied showed supramolecular columnar nematic or hexatic columnar nematic phase, which arose from the parallel alignment of the polymer supramolecular rods. The diameter of the cylindrical building block increased with increasing the length of the oligo(oxyethylene) groups. The macromolecular rod surface can be further tuned by complexation the oligo(oxyethylene) with lithium salts. Detailed study showed that this complexation also tremendously affected the liquid crystalline phase of the polymer.

1. Introduction

Soft matter self-assembly is an essential part of nanotechnology and it offers one of the few practical strategies for making nanoscale ensembles [1–5]. By tuning the shape and chemical nature of soft matter, complex structures can be achieved. A large number of exotic molecular assembly systems, including mushrooms and amphiphilic discs, have been designed. Shape and chemistry tunability is crucial to designing molecular building blocks for targeted soft matter. For example, for an ideal rod-forming system, shape parameters, such as length, diameter, and rigidity of the rods, chemistry of the core as well as the shell, can be easily tuned by judicious selection of the chemical synthesis strategy and proper molecular design; hence the self-assembly behavior of rods can be thoroughly investigated. Of interest is that many of these designing strategies are biomimetic because synthetic molecular rods share many similarities with their natural counterparts [6–10].

From a synthetic standpoint, it is challenging to design and synthesize an ideal "rod" mentioned above. Some rod parameters, such as rod length, can be readily controlled by tuning the polymer molecular weight (MW). Others, such as rod diameter and surface chemistry, cannot be easily controlled in many rod-forming systems. As a model rod-shaped polymer, mesogen-jacketed liquid crystalline polymer (MJLCP) offers a good opportunity to tune all the aforementioned structural parameters (Scheme 1) [11–13]. Based on previously reported work, in an MJLCP, the laterally attached mesogens are nearly perpendicular to the rod axes [14,15]. Because the spacer is short, the rigid mesogens intimately wraps the backbone, hence the whole polymer chain exhibits a semirigid rod feature [16,17]. From Scheme 1, it is evident that the rod length can be controlled by the MW of the MJLCPs [6]. Moreover, the diameter and surface chemistry of the rod can be tuned by altering the structure of laterally attached mesogens. For instance, when the

* Corresponding author. Tel.: +1 215 895 2083; fax: +1 215 895 6760.
** Corresponding author. Tel.: +86 10 62751726; fax: +86 10 62751708.
E-mail addresses: chirsli@drexel.edu (C.Y. Li), qfzhou@pku.edu.cn (Q. Zhou).

0032-3861/$ – see front matter © 2010 Elsevier Ltd. All rights reserved.
doi:10.1016/j.polymer.2010.05.051

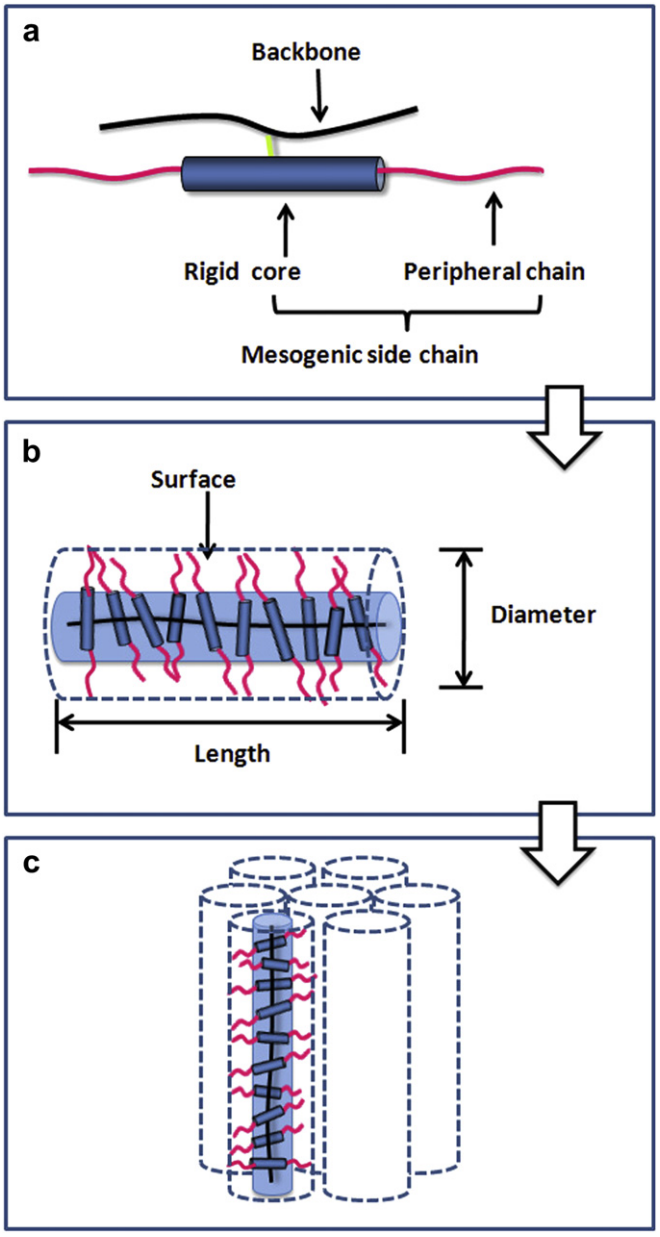

Scheme 1. Schematic illustration of Mesogen-jacketed Liquid Crystalline Polymers (MJLCPs): (a) The general molecular structure of MJLCP containing polymer backbone and laterally attached mesogenic side-chains, which composed of with the rigid-core and flexible peripheral chains; (b) The jacketing effect renders the polymer chain a semirigid rod feature. The shape parameters of the rod, including diameter, length, and surface chemistry, are related to the laterally attached mesogenic chain; (c) Supramolecular columnar phase structure is frequently observed in MJLCP system, due to parallel alignment of these semirigid polymer chains.

side attached mesogen contains three phenyl rings, the rod diameter is around 2 nm. When the side attached mesogen contains five phenyl rings, the rod diameter reaches ~3–4 nm [18].

Surface chemistry of the rod could be controlled by the substituted peripheral groups. In the previously reported MJLCP systems, the flexible terminal groups connecting to the mesogens are nonpolar alkyl chains. Oligo(oxyethylene)s, exhibiting not only polarity, but also flexibility, hydrophilicity, and the ability to form complexation with Li^+, have been used in molecular engineering of rigid rod-like conjugated polymer systems, in order to improve solubility in hydrophilic solvents [19], or to obtain "hairy rod" polymers for polymer electrolyte applications [20,21]. However, they have not been used as peripheral groups in MJLCP systems. As shown in Scheme 2, employing oligo(oxyethylene) in MJLCPs can directly lead to core-shell macromolecular rods with hydrophilic shells; these rods are significantly different from all the previously reported MJLCPs. Moreover, oligo(oxyethylene) could affect the overall phase behavior of the LCP in two ways. First, The *gauche* conformation oligo(oxyethylene) makes its cross-sectional area [22] larger than that of a normal calamitic mesogen (0.21–0.22 nm^2). This cross section mismatch could destabilize mesogen close packing in calamitic LCs [23]. However, in MJLCP systems, since the mesophase is formed because of supramolecular self-assembly of the entire polymer chains, replacement of alkyl groups by oligo(oxyethylene) might not affect the mesophase formation as significantly. Secondly, complexation of oligo (oxyethylene) with lithium salts could offer us more opportunities to tune the mesophase structure and to build up multi-functional systems based on MJLCPs. It should be noted that if fluorocarbonyl groups or oligosiloxane chains partially substitutes aliphatic chains in side-on side chain liquid crystalline polymer (SCLCP) systems [24–28], the incompatibility of fluorocarbonyl group or oligosiloxane chain with central aromatic core would finally induce the mesophase transformation from nematic phase, a predominant mesophase structure existed in side-on SCLCP, to smectic phase, indicating the chemical structure of flexible peripheral chain is important to the mesophase formation. So the question is how oligo(oxyethylene) groups influence the phase behavior of an MJLCP shown in Scheme 2.

It is the goal of this paper to investigate LC phase behaviors of a series of MJLCPs with oligo(oxyethylene) chain as flexible tails of the jacketed mesogens. In order to compare with reported MJLCP systems having alkyl chain as the mesogen tails, we used the same polyethylene backbone in our new series and kept the mesogenic core structure identical to that of the reported systems. The repeating unit number of oxyethylene group was varied from 1 to 4. The target polymer structure was listed in Scheme 2.

2. Experimental section

2.1. Materials

The compound of vinylterephthalic acid was synthesized using the method previously reported [29,30]. Chlorobenzene was purified by washing with concentrated sulfuric acid to remove thiophene, followed by washing with water, and then dried and distilled. Cuprous bromide (CuBr) was purified by stirring in glacial acetic acid, filtering, and washing with ethanol and was then dried under vacuum. 4-(Dimethylamino)pyridine (DMAP) (99%, Acros) 1-bromoethylbenzene (BEB) (97%, Acros), *N*,*N*,*N*′,*N*″,*N*″-pentamethyldiethylenetriamie (PMDETA) (>98%, TCI), 1-bromooctane (99%, J&KCHEMICA), tri(ethylene glycol) monomethyl ether (97%, Acros), tetra(ethylene glycol) monomethyl ether (99%, Aldrich), and other reagents (Beijing Chemical Works) were used as received without further purification.

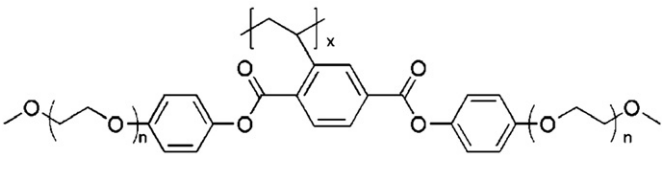

PnEOPCS, n=1-4

Scheme 2. Chemical structure of PnEOPCS (n = 1–4).

2.2. Equipments and measurements

^{1}H NMR (400 Hz) was recorded on a Bruker ARX 400 spectrometer with deuterated chloroform ($CDCl_3$) as the solvent and teramethylsilane (TMS) as the internal standard.

Elemental analyses were recorded on an Elementar Vario EL instrument.

The number-average molecular weight (M_n), weight-average molecular weight (M_w), and polydispersity index (PDI, M_w/M_n) of the resultant polymers were estimated on a gel permeation chromatography (GPC) instrument equipped with a Waters 515 HPLC pump and a Waters 2410 refractive-index detector. Three Waters Styragel columns with a 10-μm bead size were connected in series. Their effective MW ranges were 100–10,000 for Styragel HT2, 500–30,000 for Styragel HT3, and 5000–600,000 for Styragel HT4. The pore sizes were 50, 100, and 1000 nm for Styragels HT2, HT3, and HT4, respectively. THF was used as the eluent at a flow rate of 1.0 mL/min and the experiment was conducted at 35 °C. The calibration curve was constructed with polystyrene standards.

The thermal transitions of monomers and polymers were detected using a TA DSC Q100 calorimeter with a programmed heating procedure in nitrogen. The temperature and heat flow were calibrated using standard materials (indium and zinc) at different cooling and heating rates. Samples with a typical mass of 3–10 mg were encapsulated in sealed aluminum pans. A controlled cooling experiment was always carried out first, and a subsequent heating was performed at a rate that was equal to or faster than the previous cooling. Thermogravimetric analyses (TGA) was performed on a TA SDT 2960 instrument in nitrogen atmosphere using a heating rate of 20 °C/min.

One-dimensional wide-angle X-ray diffraction (1-D WAXD) powder experiments were performed on a Philips X'Pert Pro diffractometer with a 3 kW ceramic tube as the X-ray source (Cu Kα) and an X'celerator detector. The sample stage was set horizontally. The reflection peak positions were calibrated with silicon powder ($2\theta > 15°$) and silver behenate ($2\theta < 10°$). Background scattering was recorded and subtracted from the sample patterns. A temperature control unit (Paar Physica TCU 100) in conjunction with the diffractometer was utilized to study the structure evolutions as a function of temperature. The heating and cooling rates in the WAXD experiments were 10 °C/min. Two-dimensional wide-angle X-ray diffraction (2-D WAXD) was carried out using a Bruker D8 Discover diffractometer with GADDS as a 2-D detector in the transmission mode. The X-ray sources (Cu Kα) were provided by 3- kW ceramic tubes, and the diffraction peak positions were calibrated with silicon powder ($2\theta > 15°$) and silver behenate ($2\theta < 10°$). The oriented samples were prepared by mechanically shearing from the LC phase when applicable. The point-focused X-ray beam was aligned either perpendicular or parallel to the mechanical shearing direction. For both the 1-D and 2-D experiments, the background scattering was recorded and subtracted from the sample patterns. Mesophase textures were examined on a Nikon LV100 POL polarized light microscopy (PLM) with an Instec HCS302 cold and hot stage. The PLM samples were obtained using small amounts of the polymers which were melt-pressed between two cover glasses.

2.3. Synthesis of monomers nEOPCS

The chemical structures and synthesis of {2,5-bis[4-methoxyoligo(oxyethylene)phenyl]oxycarbonyl}styene (nEOPCS) are showed in Scheme 3. The experimental details are described below (taking 1EOPCS as an example).

2.4. Synthesis of 2-methoxyethyl 4-methylbenzenesulfonate

2-Methoxyethyl 4-methylbenzensulfonate was synthesized according to the literature [31].

2.5. Synthesis of 4-methoxyethoxyphenol

2-Methoxyethyl 4-methylbenzensulfonate (2.30 g, 0.01 mol), hydroquinone (2.20 g, 0.02 mol), and excess KOH were dissolved in 200 mL ethanol. The reaction mixture was heated to reflux under argon. After 24 h, the reaction mixture was cooled to room temperature. The solution was concentrated by rotary evaporation, mixed with 50 mL water, and then acidified to pH = 2 using HCl. The mixture was extracted by dichloromethane. The dichloromethane was removed by rotary evaporation to yield a crude product. The crude product was recrystallized in petroleum ether/ethyl acetate to yield a white solid product (0.53 g, yield: 31%).

2.5.1. 2,5-Bis[4-(methoxyethoxyphenyl)oxycarbonyl]styrene (1EOPCS)

4-Methoxyethoxyphenol (1.68 g, 0.01 mol), *N*,*N*′-dicyclohexylcabodiimide (DCC) (2.06 g, 0.01 mol), 4-(dimethylamino)pridine (DMAP) (0.17 g, 0.001 mol), and vinylterephthalic (1.15 g, 0.006 mol) were dissolved in 60 mL of dichloromethane. The mixture was stirred for 8 h at room temperature. Then the salt was removed by filtration and the solvent was removed by rotary evaporation. A yellow solid product was obtained. The solid was recrystallized with methanol to yield a white solid product (1.04 g, yield: 42%). ^{1}H NMR (δ, $CDCl_3$, ppm): 8.43–8.42 (d, 1H, Ar–*H*), 8.21–8.15 (m, 2H, Ar–*H*), 7.58–7.51 (q, 1H, –*CH*=CH_2), 7.16–7.14 (d, 2H, Ar–*H*), 6.98–6.96 (d, 2H, Ar–*H*), 5.86–5.81 (d,1H, –CH=*CH*$_2$), 5.50–5.47 (d, 1H, –CH=*CH*$_2$), 4.16–4.13 (m, 4H, –O*CH*$_2$–*CH*$_2$O–), 3.79–3.76 (t, 4H, –O*CH*$_2$–*CH*$_2$O–), 3.40 (s, 6H, –O*CH*$_3$). ^{13}C NMR (δ, $CDCl_3$, ppm): 59.18–59.23 (–OCH_3), 67.73 (Ar–OCH_2–), 70.97 (Ar–OCH_2CH_2O–), 115.27 (aromatic *C* ortho to –$OCH_2CH_2OCH_3$), 118.42 (–CH=CH_2), 122.29 (aromatic *C* meta to –$OCH_2CH_2OCH_3$), 128.62 (aromatic *C* ortho to –CH=CH_2 and –C=O), 129.00 (aromatic *C* para to –CH=CH_2), 130.91 (aromatic *C* meta to –CH=CH_2 and ortho to –C=O), 131.91 (–*C*H=CH_2), 133.14–134.64

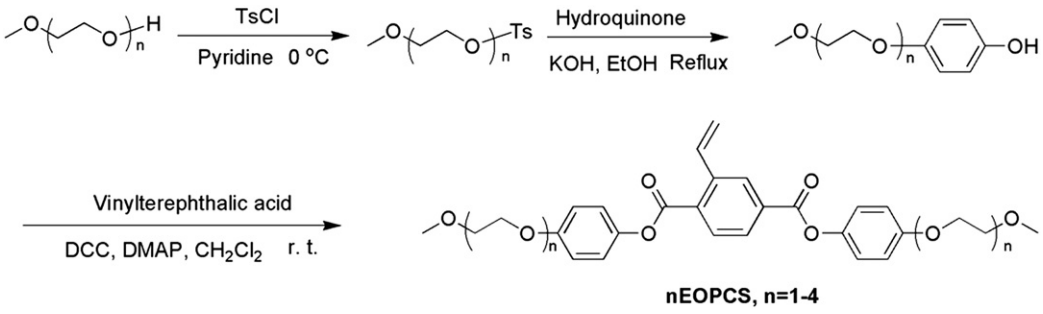

Scheme 3. Synthesis of the monomers nEOPCS (n = 1–4).

(aromatic *C*–C=O), 140.43 (aromatic *C*–CH=CH_2), 144.26–144.37 (aromatic *C*–O–C=O), 156.70 (aromatic *C*–O $CH_2CH_2OCH_3$), 164.54–165.31 (*C*=O). Elemental Analysis: Found (Calc.): C 68.21 (68.28); H 5.62 (5.73). MS (EI): $M^+ = 492$.

2.5.2. 2,5-Bis{4-[methoxydis(oxyethylene)phenyl]oxycarbonyl} styrene (2EOPCS)

The synthetic procedure was the same as that for 1EOPCS except that 4-methoxybis(oxyethylene)phenol was used instead of 4-methoxyethoxyphenol. ^{1}H NMR (δ, $CDCl_3$, ppm): 8.44–8.43 (d,1H, Ar–*H*), 8.22–8.16 (m, 2H, Ar–*H*), 7.58–7.51 (q, 1H, –*CH*=CH_2), 7.16–7.14 (q, 4H, Ar–*H*), 6.99–6.97 (q, 4H, Ar–*H*), 5.86–5.82 (d, 1H, –CH=C*H*$_2$), 5.50–5.47 (d, 1H, –CH=C*H*$_2$), 4.18–4.15 (m, 4H, Ar–OC*H*$_2$–CH_2O–), 4.00–3.87 (m, 4H, Ar–OCH_2–C*H*$_2$O–), 3.57–3.73 (m, 4H, Ar–OCH_2–CH_2O–C*H*$_2$–CH_2O–), 3.60–3.59 (m, 4H, Ar–OCH_2–CH_2O–CH_2–C*H*$_2$O–), 3.40 (s, 6H, -OC*H*$_3$). ^{13}C NMR (δ, $CDCl_3$, ppm): 59.18–59.23 (-OCH_3), 67.78 (Ar–OC*H*$_2$–), 69.62 (Ar–OCH_2C*H*$_2$O–), 70.66 (–$OCH_2CH_2OCH_3$), 71.84 (–$OCH_2CH_2OCH_3$), 115.27 (aromatic *C* ortho to –$OCH_2CH_2OCH_3$), 118.42 (–CH=C*H*$_2$), 122.29 (aromatic *C* meta to –$OCH_2CH_2OCH_3$), 128.62 (aromatic *C* ortho to –CH=CH_2 and –C=O), 129.00 (aromatic *C* para to –CH=CH_2), 130.91 (aromatic *C* meta to –CH=CH_2 and ortho to –C=O), 131.91 (–*C*H=CH_2), 133.14–134.64 (aromatic *C*–C=O), 140.43 (aromatic *C*–CH=CH_2), 144.26–144.37 (aromatic *C*–O–C=O), 156.70 (aromatic *C*–O $CH_2CH_2OCH_3$), 164.54–165.31 (*C*=O). Elemental Analysis: Found (Calc.): C 66.12 (66.19); H 6.16 (6.25). MS (EI): $M^+ = 580$.

2.5.3. 2,5-Bis{4-[methoxytris(oxyethylene)phenyl]oxycarbonyl} styrene (3EOPCS)

The synthetic procedure was the same as that for 1EOPCS except that 4-methoxytris(oxyethylene)phenol was used instead of 4-methoxyethoxyphenol. ^{1}H NMR (δ, $CDCl_3$, ppm): 8.45–8.44 (d,1H, Ar–*H*), 8.22–8.17 (m, 2H, Ar–*H*), 7.59–7.52 (q, 1H, –*CH*=CH_2), 7.16–7.14 (q, 4H, Ar–*H*), 6.99–6.96 (q, 4H, Ar–*H*), 5.85–5.82 (d, 1H, –CH=C*H*$_2$), 5.51–5.47 (d, 1H, –CH=C*H*$_2$), 4.20–4.17 (m, 4H, Ar–OC*H*$_2$–CH_2O–), 3.91–3.90 (m, 4H, Ar–OCH_2–C*H*$_2$O–), 3.78–3.56 (m, 12H, Ar–OCH_2CH_2–OC*H*$_2$C*H*$_2$OC*H*$_2$$CH_2$–), 3.58–3.56 (m, 4H, Ar–$OCH_2CH_2OCH_2CH_2OCH_2$C*H*$_2$–), 3.40 (s, 6H, OCH_3). ^{13}C NMR (δ, $CDCl_3$, ppm): 58.66 (OCH_3), 67.22 (Ar–OCH_2CH_2O–), 69.47 (Ar–OCH_2C*H*$_2$O–), 70.22–70.51 (Ar$OCH_2CH_2OCH_2CH_2OCH_2$-CH_2OCH_3), 71.56 (–OCH_2C*H*$_2$$OCH_3$), 115.03 (aromatic *C* ortho to –OCH_2CH_2), 118.48 (–CH=C*H*$_2$), 122.04 (aromatic *C* ortho to –O–C=O), 128.67 (aromatic *C* ortho to –CH=CH_2 and –C=O), 129.04 (aromatic *C* para to –CH=CH_2), 130.91 (aromatic *C* meta to –CH=CH_2 and ortho to –C=O), 132.01 (–*C*H=CH_2), 133.14–134.64 (aromatic *C*–C=O), 140.43 (aromatic *C*–CH=CH_2), 144.24–144.39 (aromatic *C*–O–C=O), 156.70 (aromatic *C*–O $CH_2CH_2OCH_3$), 164.64–165.51 (*C*=O). Elemental Analysis: Found (Calc.): C 63.48 (63.52); H 6.93 (6.90). MS (EI): M+ = 648.

2.5.4. 2,5-Bis{4-[methoxytetra(oxyethylene)phenyl]oxycarbonyl} styrene (4EOPCS)

The synthetic procedure was the same as that for 1EOPCS except that 4-methoxytetra(oxyethylene)phenol was used instead of 4-methoxyethoxyphenol. ^{1}H NMR (δ, $CDCl_3$, ppm): 8.43–8.42 (d,1H, Ar–*H*), 8.22–8.17 (m, 2H, Ar–*H*), 7.55–7.49 (q, 1H, –*CH*=CH_2), 7.16–7.14 (q, 4H, Ar–*H*), 6.99–6.96 (q, 4H, Ar–*H*), 5.86–5.80 (d, 1H, –CH=C*H*$_2$), 5.50–5.46 (d, 1H, –CH=C*H*$_2$), 4.17–4.15 (m, 4H, Ar–OC*H*$_2$–CH_2O–), 3.89–3.87 (m, 4H, Ar–OCH_2–C*H*$_2$O–), 3.75–3.61 (m, 20H, Ar–OCH_2CH_2–OC*H*$_2$C*H*$_2$OC*H*$_2$C*H*$_2$ OC*H*$_2$$CH_2$–), 3.58–3.56 (m, 4H, Ar–$OCH_2CH_2OCH_2CH_2OCH_2$C*H*$_2$–), 3.35 (s, 6H, OCH_3). ^{13}C NMR (δ, $CDCl_3$, ppm): 58.90 (OCH_3), 67.43 (Ar–OCH_2CH_2O–), 67.78 (Ar–OC*H*$_2$C*H*$_2$O–), 69.57.39–70.73 (ArOCH_2CH_2O(CH_2C*H*$_2$)$_2$O$CH_2CH_2OCH_3$), 71.81 (–OCH_2C*H*$_2$$OCH_3$), 115.24 (aromatic *C* ortho to –OCH_2CH_2), 118.31 (–CH=C*H*$_2$), 122.18 (aromatic *C* ortho to –O–C=O) 128.52 (aromatic *C* ortho to –CH=CH_2 and –C=O), 128.91 (aromatic *C* para to –CH=CH_2), 130.81 (aromatic *C* meta to –CH=CH_2 and ortho to –C=O), 131.80 (–*C*H=CH_2), 133.03–134.52 (aromatic *C*–C=O), 140.37 (aromatic *C*–CH=CH_2), 144.10–144.20 (aromatic *C*–O–C=O), 156.62 (aromatic *C*–O $CH_2CH_2OCH_3$), 164.42–165.19 (*C*=O). Elemental Analysis: Found (Calc.): C 62.18 (63.48); H. 6.86 (6.93) MS (EI): $M^+ = 756$.

2.6. Polymerization

Polymers were obtained either by conventional solution radical polymerization or by atom transfer radical polymerization (ATRP). A typical polymerization procedure by conventional solution radical polymerization is summarized as the following. About 1EOPCS (0.4 g, 0.8 mol), 40 μL of 0.05M BPO chlorobenzene solution, and 2 mL of chlorobenzene were transferred into a polymerization tube. After three freeze–pump–thaw cycles, the tube was sealed under vacuum. Polymerization was carried out at 60 °C for 24 h. The tube was then opened and the reaction mixture was diluted with 10 ml THF. After evaporation of the solvent, the products were purified using column chromatography with dichloromethane as the eluent in order to remove unreacted monomers. Polymers were obtained by precipitation in methanol followed by drying under vacuum at room temperature for 24 h.

A typical polymerization procedure by ATRP is summarized as the following. 1EOPCS (0.25 g, 0.5 mmol), BEB (1.85 mg, 0.1 mmol), PMDETA (1.73 mg, 0.1 mmol), and chlorobenzene (4 g) were added sequentially into a reaction tube containing a magnetic stir bar. The reaction mixture was purged with nitrogen and was subjected to two freeze–thaw cycles to remove any dissolved oxygen. Then CuBr (1.44 mg, 0.1 mmol) was added into the reaction tube. After another two freeze–thaw cycles, the tube was sealed under vacuum. Polymerization was carried out at 90 °C for 24 h. After the polymerization was terminated by immersing the tube into cold water, the tube was broken. The polymerization mixture was then diluted with 20 mL THF, and was passed through an Al_2O_3 column to remove the copper complex. The solution was concentrated by rotary evaporation and purified by silica gel column chromatography with dichloromethane as the eluent. The solution was precipitated using methanol. The precipitate was dried under vacuum. The molecular weight and polydispersity of the polymer were measured by GPC with PS standards.

Table 1
Polymerization results of PnEOPCS.

Sample	M_n[a] ($\times 10^4$ g/mol)	PDI[a]	Liquid Crystallinity[b]
P1EOPCS-1	2.69	1.32	No
P1EOPCS-2	3.08	1.27	No
P1EOPCS-3	4.44	1.27	Yes
P1EOPCS-4	4.47	1.24	Yes
P1EOPCS-5	5.89	1.24	Yes
P1EOPCS-6	11.4	1.65	Yes
P2EOPCS-1	2.0	1.18	No
P2EOPCS-2	10.1	1.50	Yes
P3EOPCS-1	2.45	1.20	No
P3EOPCS-2	12.7	1.65	Yes
P4EOPCS-1	4.1	1.60	No
P4EOPCS-2	9.7	1.99	Yes

[a] Molecular weights and polydispersity were measured by GPC, using terahydrofuran as an eluent at 35 °C and monodisperse polystyrene as the standard.
[b] Determined from PLM.

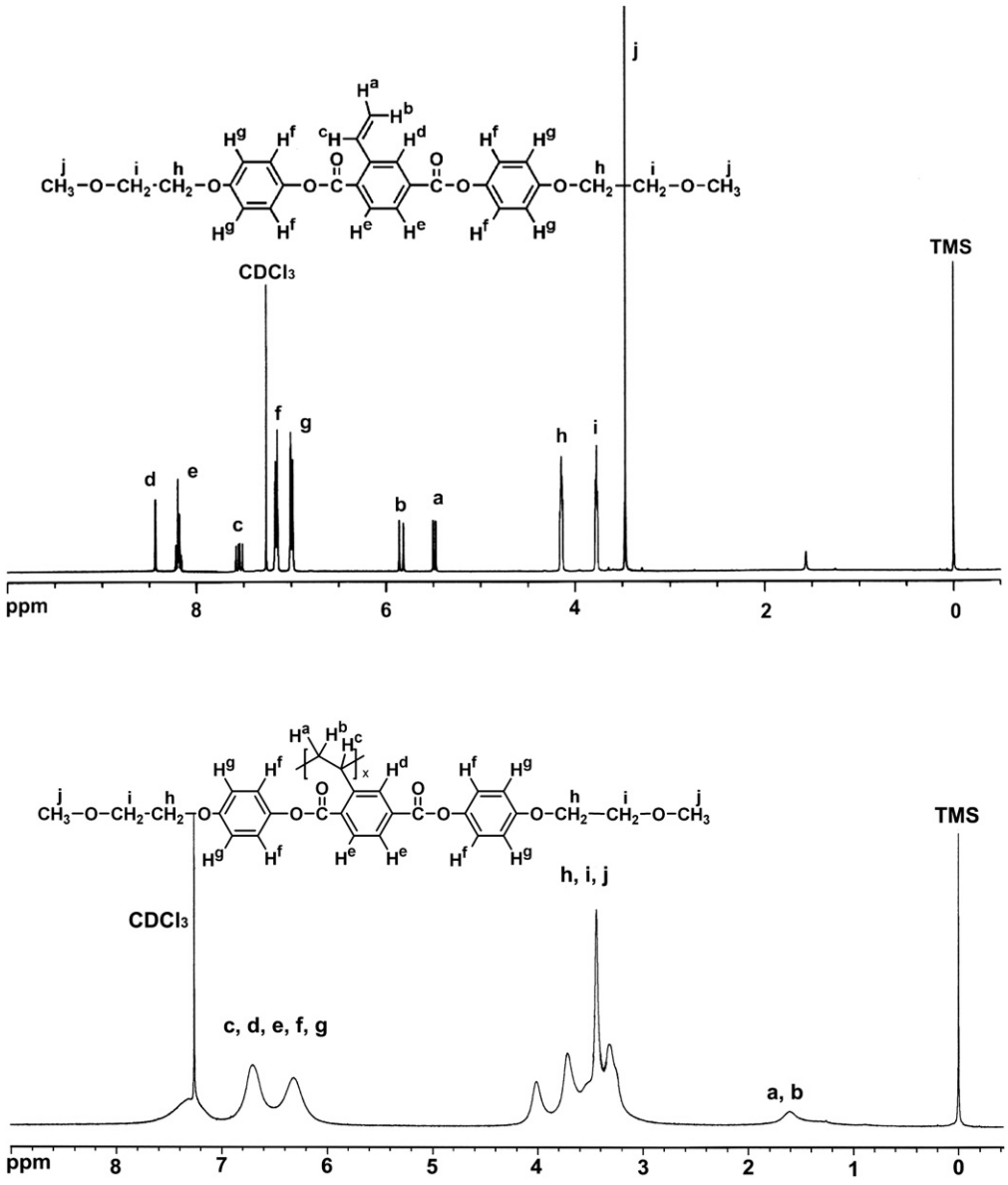

Fig. 1. ^{1}H NMR spectra of 1EOPCS and P1EOPCS in $CDCl_3$, respectively.

3. Results and discussion

3.1. Synthesis of monomers

Monomers were synthesized by the reaction of 2-vinylterephthalic acid and 4-methoxyoligo(oxyethylene)phenol in the presence of DCC and DMAP in CH_2Cl_2. All monomers were thoroughly purified by silica gel column chromatography. 1EOPCS was further purified by recrystallization. The resulting monomer molecular structures were confirmed by ^{1}H NMR, ^{13}C NMR, mass spectroscopy and elemental analysis. All of the monomers were stored in refrigerator before use.

3.2. Polymerization

Both ATRP and conventional free radical polymerization were conducted to synthesize polymer samples with different MWs. For polymer samples with MW $> 10 \times 10^4$ g/mol, conventional free radical polymerization was employed while ATRP was used to obtain samples with MW$<10 \times 10^4$ g/mol. MW and polydispersity of all the polymers are listed in Table 1. PnEOPCS have good solubility in common organic solvents such as THF and chloroform. Conversion and purification of polymers were confirmed by ^{1}H NMR spectroscopy and GPC. As an example, Fig. 1 shows the ^{1}H NMR spectra of monomer 1EOPCS and polymer P1EOPCS. 1EOPCS showed characteristic resonances of the vinyl group at 5.5–5.9 and 7.5–7.6 ppm. After polymerization, the signals disappeared completely. The adsorption peaks of P1EOPCS are quite broad, which is consistent with the expected polymer structure.

3.3. Mesomorphic properties of the monomers

Among all the monomers synthesized, 3EOPCS and 4EOPCS are liquid at the room temperature. 2EOPCS is crystalline with a melting temperature of 40 °C. Thermal behavior of 1EOPCS was examined using PLM. Above the melting point (72 °C), the sample became isotropic. Nematic droplets and typical Schlieren textures were only observed upon cooling from isotropic melt, indicating

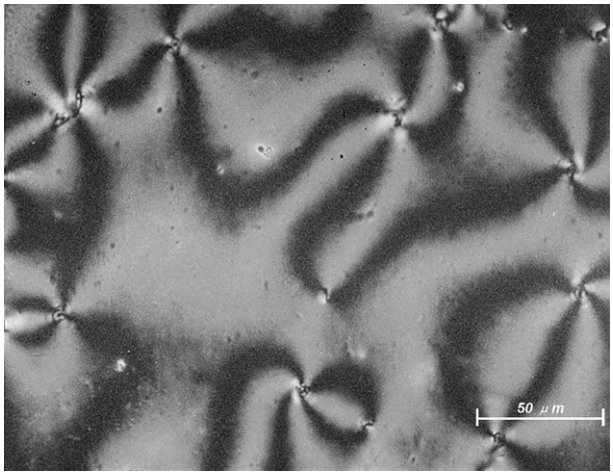

Fig. 2. Schlieren textures of 2,5-bis[4-(methoxyethoxybenzene)oxycarbonyl]styrene (1EOPCS) observed at 70 °C under polarized light microscopy during cooling from isotropic melt.

the formation of the monotropic nematic phase (Fig. 2). Nematic phase was frequently observed in MJLCP monomers because the laterally attached vinyl group tends to hinder the hard cores to tightly pack together. The existence of oligo(ethyleneoxy) chain, in this case, further decreased the melting point, mesophase temperature range, and isotropization point, which is similar to the reported calamitic LC systems [23].

3.4. Mesomorphic properties of the polymers

As shown in Table 2, all the polymers are quite thermally stable because the temperature of 1% weight loss under nitrogen atmosphere is above 290 °C. DSC, PLM, and WAXD experiments were all carried out under inert atmosphere below 290 °C. Therefore, thermal degradation will not be considered in the following discussions on the liquid crystalline behavior of the polymers.

Both heating and cooling DSC traces of the polymers show glass transitions of the polymers (Fig. 3). No clear first order transitions were observed, which is characteristic for most MJLCPs reported [30,32–34]. The glass-transition temperatures (T_g) listed in Table 2 were estimated from the second-heating DSC curves of the polymers. Upon increasing n from 1 to 4, T_g decreased from 86 °C to −36 °C, which can be attributed to the high conformational entropy of the oligo(oxyethylene) tails.

Liquid crystallinity of samples with different MWs was examined under PLM. For low M_n samples ($M_n < 4.0 \times 10^4$ g/mol), no birefringence was observed under PLM in the temperature region studied, irrespective of various thermal histories (including heating, cooling, and isothermal annealing). For the samples with high and intermediate M_n values, as-cast films did not show

Table 2
Molecular characteristics and phase transition temperatures of PnEOPCS.

Polymer	M_n[a] ($\times 10^4$ g/mol)	PDI[a]	T_g[b] (°C)	T_d[c] (°C)
P1EOPCS	11.4	1.65	86	292
P2EOPCS	10.1	1.50	54	294
P3EOPCS	12.7	1.65	32	289
P4EOPCS	9.7	1.99	-36	290

[a] Molecular weights and polydispersity were measured by GPC, using terahydrofuran as the eluent at 35 °C and monodisperse polystyrene as the standard.
[b] Glass transition temperature, determined from the second-heating DSC curves at a rate of 10 °C/min.
[c] The temperature at which 1% weight loss of the sample was reached from TGA under nitrogen atmosphere.

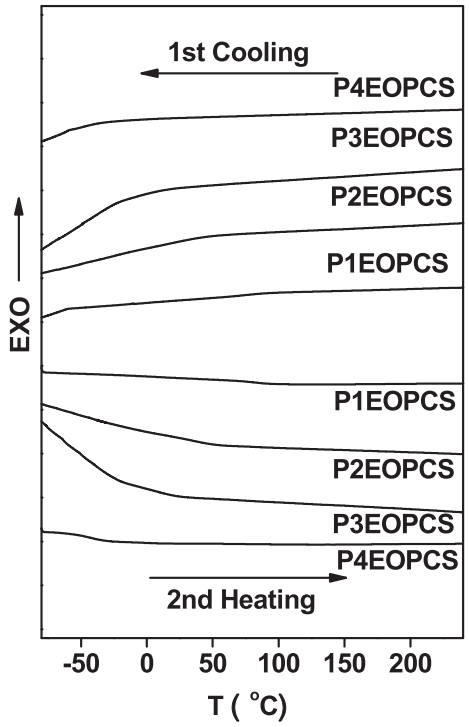

Fig. 3. DSC curves of PnEOPCS ($n = 1$–4) during second-heating scan and first cooling scan at a rate of 10 °C/min under a N_2 atmosphere.

birefringence. The powder sample, however, exhibited weak birefringence because of the presence of a low degree of mesomorphic order, which had been formed during precipitation of the polymer. Upon heating, no immediate development of birefringence was observed for all of the polymers near T_g. The birefringence appeared and became increasingly strong after the samples reached about 160 °C. Then the LC textures retained and no visual disappearance of birefringence could be observed before the polymer decomposed. When the sample was cooled to room temperature from 290 °C, its birefringence remained unchanged, suggesting that the ordered structure formed at high temperatures was kept upon cooling. For P1EOPCS-5, schlieren texture was formed after the sample was annealed at 200 °C for half an hour without mechanical shearing, as shown in Fig. 4a. When the sample was sheared, characteristic LC banded texture with alternating birefringence was observed. Fig. 4b–d displays the banded texture of PnEOPCS ($n = 1$–3) formed after shearing at 200 °C. The banded texture of P4EOPCS was hardly formed because of its low T_g.

To further characterize phase transitions of PnEOPCS, temperature-dependent powder WAXD was used. Fig. 5 shows the WAXD results for P2EOPCS during heating and cooling scans at a rate of 10 °C/min. Over the test region of 2θ from 2° to 35°, two peaks were visible, located in the low-angle region near 5° and wide-angle region around 20°, respectively. Between 30 °C and 120 °C, the low-angle diffraction peak appeared weak and diffused, suggesting a short-range order of the polymer chain packing. At higher temperatures, P2EOPCS displayed an intense diffraction peak at $2\theta = 4.53°$, corresponding to a d-spacing of 1.95 nm. The d-spacing evolution of P2EOPCS with temperature in the low-angle region during the first heating in Fig. 6a shows a significant decline of d-spacing from 2.10 nm to 1.95 nm during heating appears around 120–160 °C, indicating an ordered structure developed during this temperature region. With increasing temperature, the intensity of this peak increased up to 250 °C, the highest temperature at which the WAXD was run. This result is consistent with the

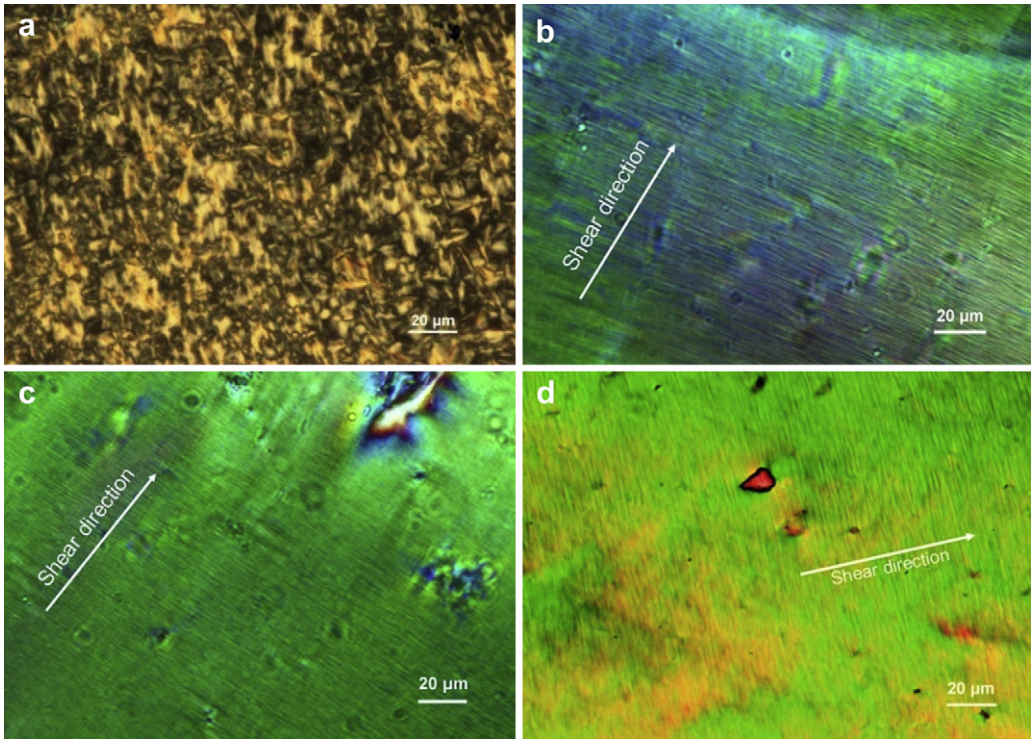

Fig. 4. Polarized light micrographs of P1EPCS-5 annealed at 200 °C (a), banded texture of P1EOPCS sheared at 200 °C (b), banded texture of P2EOPCS sheared at 190 °C (c), and banded texture of P3EOPCS sheared at 170 °C (d).

aforementioned PLM observation that the LC phase developed during the first heating was very stable at high temperatures and no LC-to-isotropic phase transition temperature could be detected before decomposition. On the subsequent cooling scan, the low-angle diffraction peak slightly weakened and gradually shifted to higher 2θ values because of thermal shrinking (Fig. 5b). However, the sharp diffraction profile retained. In the wide-angle region, for both heating and cooling scans, the diffraction peak appeared diffused and little change was observed over the entire temperature region examined, suggesting that no long-range-ordered crystalline structure had been formed *via* molecular packing on a scale of about 0.5 nm. PnEOPCS ($n = 1, 3, 4$) had similar powder WAXD patterns as those of P2EOPCS. Fig. 6 shows *d*-spacing evolution of the diffraction peak in the low-

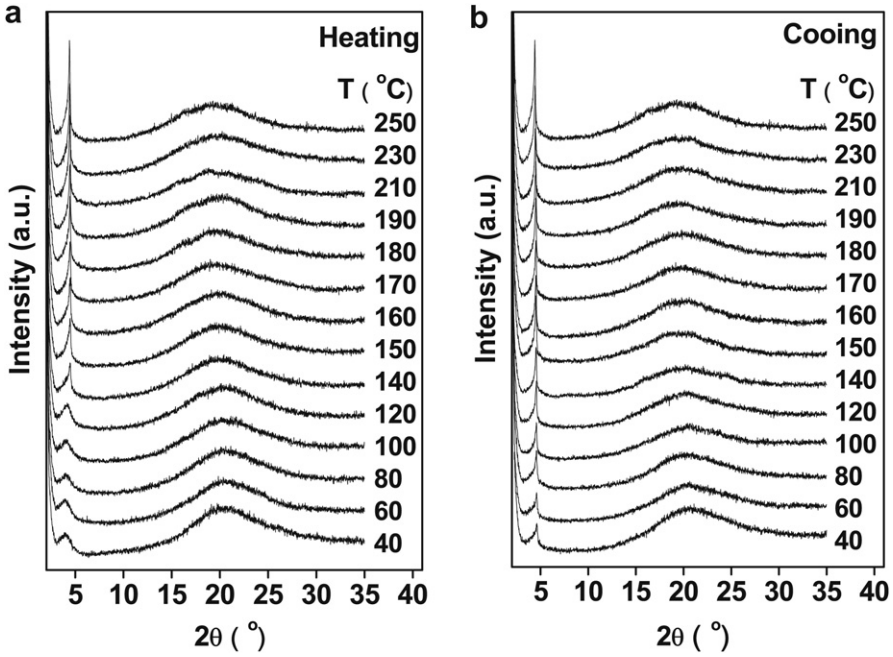

Fig. 5. Set of 1-D WAXD powder patterns of P2EOPCS obtained during the first heating of the as-cast film (a) and corresponding first cooling WAXD powder patterns of the same film (b).

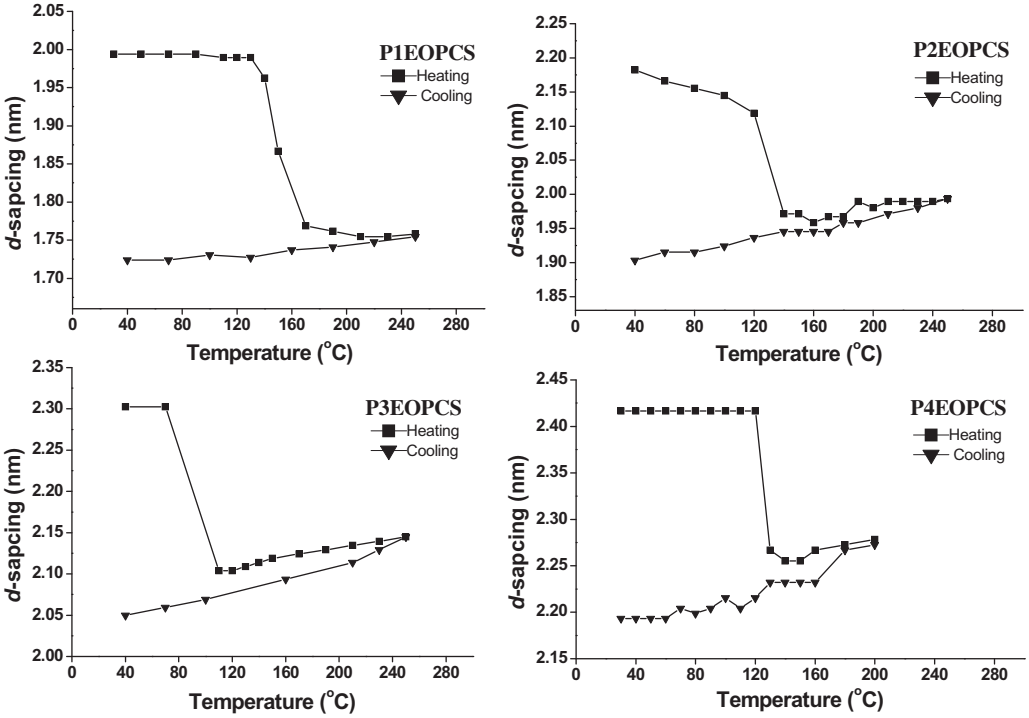

Fig. 6. *d*-Spacings of diffraction peaks of PnEOPCS as functions of temperature measured during the first heating and subsequent cooling in the low-angle region of WAXD powder patterns.

angle region of PnEOPCS as a function of temperature measured during the first heating and subsequent cooling. Similar trends are observed in all four samples. Note that although T_g of PnEOPCS decreased significantly with increasing length of flexible oligo(oxyethylene) chain, the onset temperatures of the sudden *d*-spacing drop in the figure were similar. Fig. 7a depicts a set of 1-D WAXD powder patterns for this series of PnEOPCS samples obtained at 210 °C. The *d*-spacings measured from Fig. 7a are shown in Fig. 7b as a function of *n*. The *d*-spacing increased with the *n* changed from 1 to 4, which is attributed to the increased length of the oligo(ethyleneoxy) chain.

2-D WAXD experiments were carried out to further characterize the mesomorphic phase structure. In order to achieve chain orientation, specimens were obtained by drawing fibers, or shearing films, of the polymer at the mesophase temperature. The fibers or films were annealed at the same temperature for several hours, and were then quenched to room temperature. Fig. 8a–c shows the 2-D WAXD patterns of PnEOPCS ($n = 1$–3), with the X-

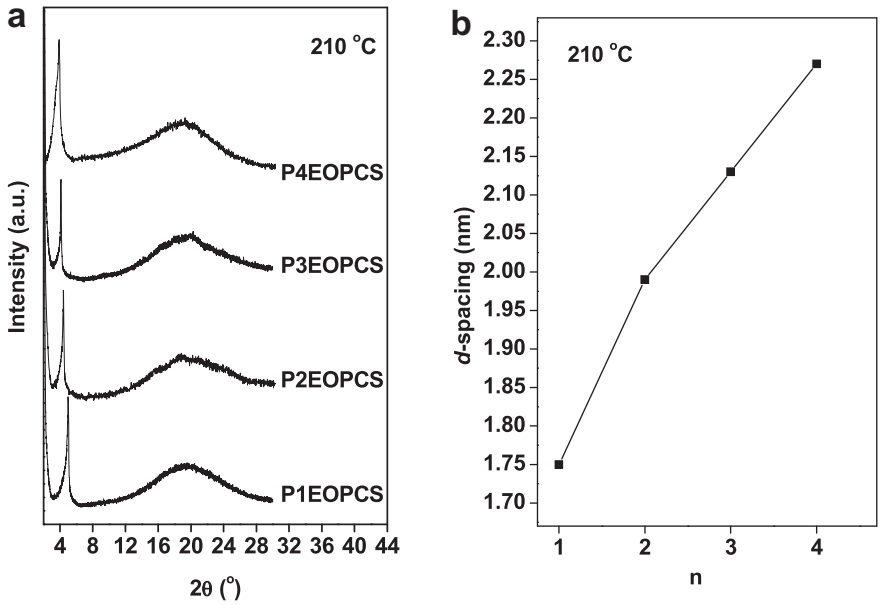

Fig. 7. Set of 1-D WAXD powder patterns for PnEOPCS samples as obtained at 210 °C (a). The *d*-spacings of diffraction peaks at in the low-angle region measured from (a) as a function of *n* (b).

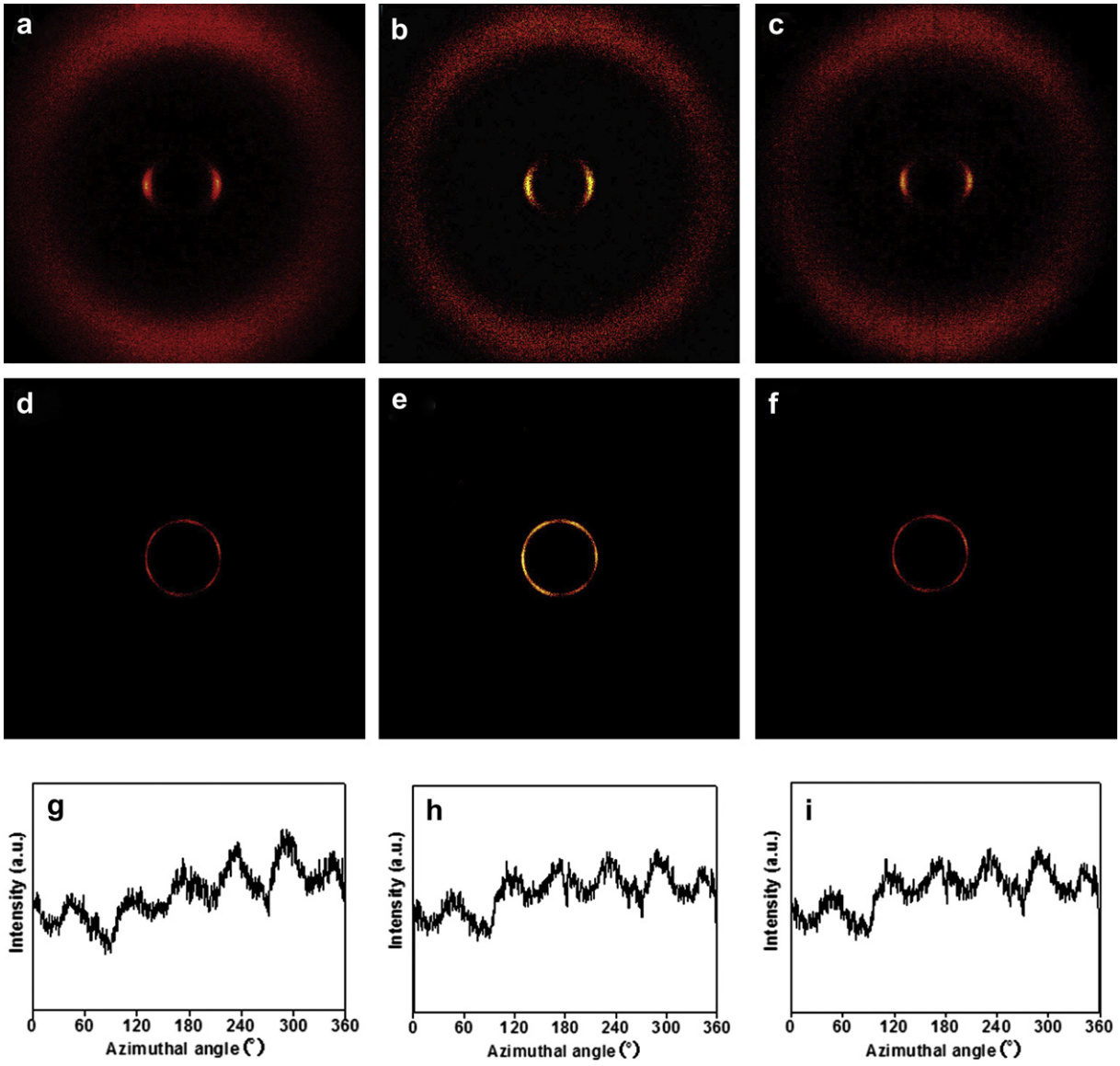

Fig. 8. 2-D WAXD fiber patterns of PnEOPCS ($n = 1$–3) obtained with the X-ray beam perpendicular to the shear direction (a: $n = 1$; b: $n = 2$; c: $n = 3$) and parallel to the shear direction (d: $n = 1$; e: $n = 2$; f: $n = 3$). The corresponding azimuthal scanning data of the low-angle diffraction of (d, e) are shown in g ($n = 1$), h ($n = 2$), and i ($n = 3$).

ray incident beam perpendicular to the fiber axis. A pair of strong diffraction arcs can be seen on the equators at $2\theta = 5.04^\circ$ (d-spacing of 1.75 nm) for P1EOPCS, $2\theta = 4.52^\circ$ (d-spacing of 1.95 nm) for P2EOPCS, and $2\theta = 4.26^\circ$ (d-spacing of 2.07 nm) for P3EOPCS, indicating that ordered structures have developed along the direction perpendicular to the fiber axis. Higher-order diffractions were not observed, even with thermal annealing. This result is consistent with 1-D WAXD patterns. On the other hand, scattering halos in the wide-angle region are concentrated on the meridians with rather broad azimuthal distributions. This reveals that only short-range order exists along the fiber direction.

Fig. 8d–f shows the 2-D WAXD patterns of PnEOPCS ($n = 1$–3), with the X-ray incident beam parallel to the fiber axis. For these samples, six diffraction arcs are located at $2\theta = 5.04^\circ$ (d-spacing of 1.75 nm) for P1EOPCS, $2\theta = 4.52^\circ$ (d-spacing of 1.95 nm) for P2EOPCS, and $2\theta = 4.26^\circ$ (d-spacing of 2.07 nm) for P3EOPCS. The corresponding azimuthal intensity profiles shown in Fig. 8g–i exhibit six maxima with an angle of 60° between the two adjacent diffraction. Maxima, although the intensities are not exactly identical (this may be caused by imperfection in the sample orientation). This indicates a hexagonal lateral packing of the cylinders with each cylinder having an average diameter of 2.02 nm for P1EOPCS, 2.22 nm for P2EOPCS, and 2.39 nm for P3EOPCS. Each cylinder is occupied by a single PnEOPCS polymer chain. Since the diameter values are smaller than the lengths of laterally attached mesogens, the side-chains wrapping around the polymer backbone are expected to tilt about 51° (take P1EOPCS as an example) away from the cylinder long axis. However, this hexagonal lateral packing lacks long-range order perpendicular to the fiber axis, since the higher-order diffractions are missing [15] [35–39]. Therefore, the ordered structure of PnEOPCS ($n = 1$–3) should be assigned as a hexatic columnar nematic (Φ_{HN}) phase. Φ_{HN} phase was further confirmed by 2-D WAXD examination of P1EOPCS sheared films, which is shown in Fig. 9. The shear geometry is shown in Fig. 9d. V, $V \times \nabla V$ and ∇V indicate shear flow, shear vorticity, and shear gradient directions, respectively.

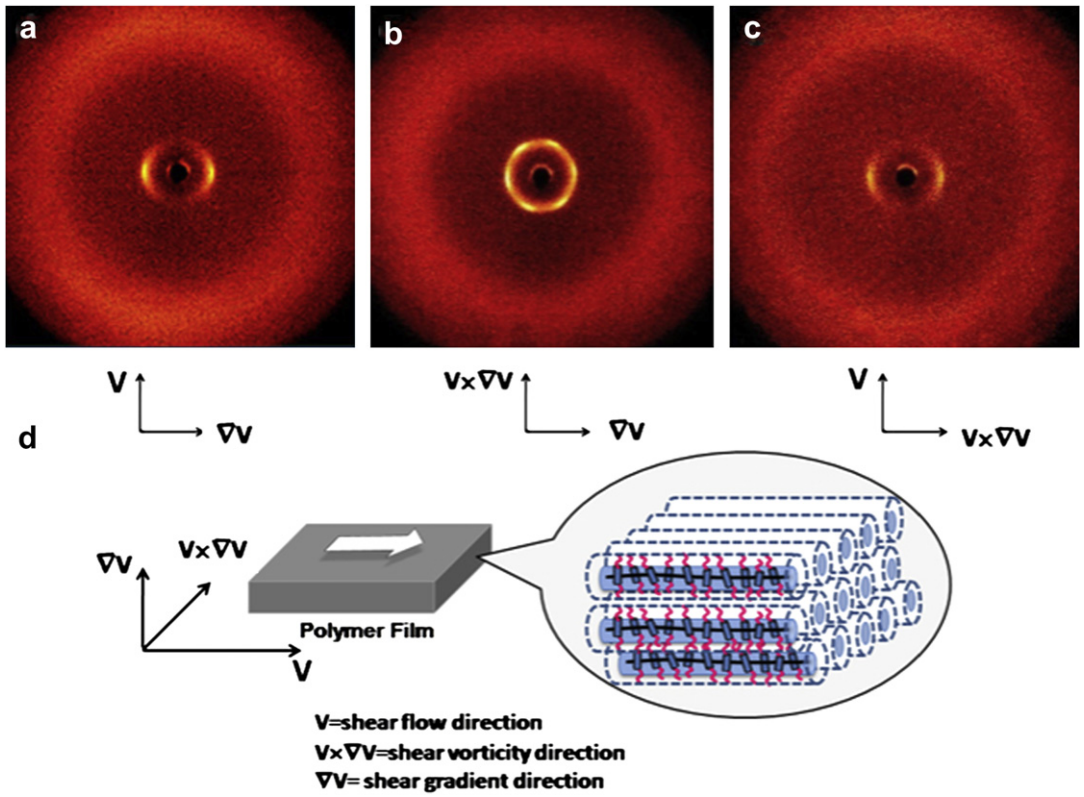

Fig. 9. 2-D WAXD of a P1EOPCS film obtained with the X-ray beam along (a) the $V \times \nabla V$, (b) the V, and (c) the ∇V direction. V is the shear direction as defined in (d) the schematic representation of the shear geometry.

When X-ray incident beam is parallel to the shear flow (V) direction, six diffraction arcs are located at $2\theta = 5.04°$, while in $V \times \nabla V$ and ∇V direction, two diffraction arcs with the same 2θ angle value are located on the equator. These characteristic 2-D diffraction patterns indicate that a uniformly oriented hexatic structure is easily achieved under mechanical shear with each cylinder parallel to the shear direction. Since each cylinder is formed by a single PnEOPCS ($n = 1–3$) chain molecule, a packing model of P1EOPCS after shearing is illustrated in part d of Fig. 9. More information about the orientation of the hexatic phase could be obtained in Fig. 9b. The diffraction falls on ∇V and 30° from $V \times \nabla V$ axis, suggesting that if a hexatic lattice cross section in (d) (head on view) was drawn, the hexagon should have an orientation that one side of the hexagon is parallel to the film surface.

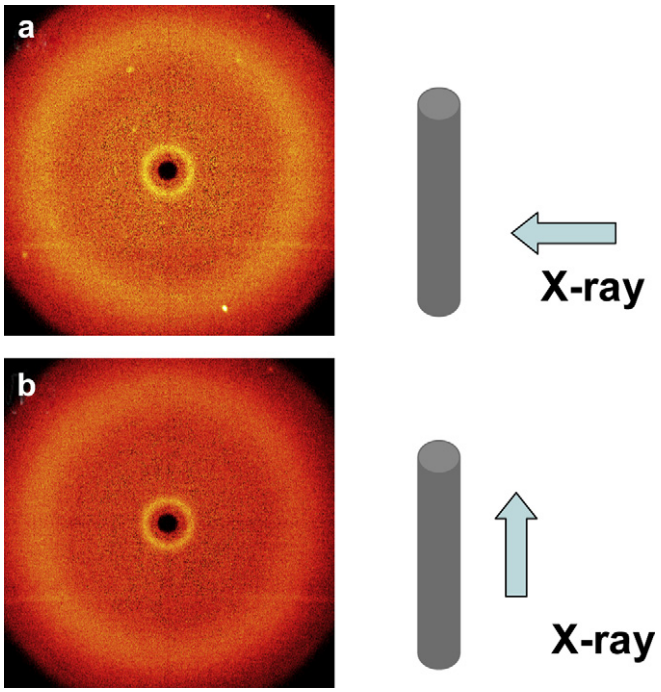

Fig. 10. 2-D WAXD patterns of P4EOPCS fiber obtained with the X-ray beam perpendicular to the shear direction (a) and parallel (b) to the shear direction.

The phase structure of P4EOPCS is, however, different from that of PnEOPCS ($n = 1–3$). 2-D WAXD experiments were conducted on both fiber and sheared film samples of P4EOPCS. Fig. 10 shows the 2-D WAXD patterns of P4EOPCS fiber with the X-ray beam perpendicular/parallel to the shear direction. In both patterns, we can only observe uniform diffraction circles at the low- and high-angle region, indicating the lack of macroscopic orientation of the sample. Furthermore, careful comparison of diffraction patterns in Fig. 7a shows that the full width at half maximum (FWHM) of the low-angle reflection peak for P4EOPCS (0.605°) is quite different from that of PnEOPCS ($n = 1–3$; 0.143° for P3EOPCS, 0.214° for P2EOPCS, and 0.270° for P1EOPCS). This dramatic difference in FWHM suggests that the LC phase is less ordered in P4EOPCS and the phase structure can be assigned as a columnar nematic phase (Φ_N).

3.5. Polymer-salt mixtures

P4EOPCS were mixed with lithium trifluoromethanesulfonate ($LiCF_3SO_3$) in various molar ratios of Li to [EO] equal to 0.0125 and 0.0625, where EO refers to oligo(oxyethylene)'s repeating unit $-CH_2CH_2O-$. Fig. 11 shows the DSC curves of the polymer-salt

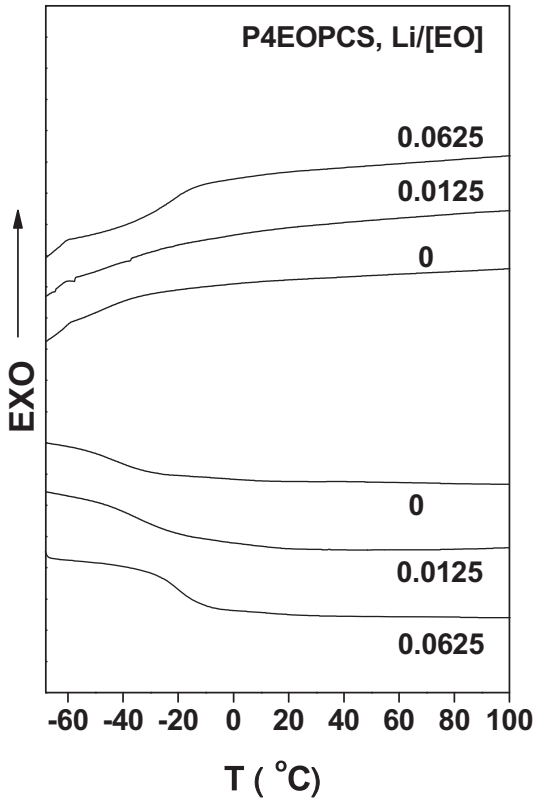

Fig. 11. DSC curves of P4EOPCS and corresponding P4EOPCS complex with lithium salts at a heating rate of 10 °C/min.

mixtures at a heating rate of 10 °C/min. It is clear that T_g increases with increasing Li^+/[EO], which is because the complexation of Li^+ and oxyethylene units restricts segmental motions. Similar effect has been found in other reported polymer/Li^+ complex systems [20,21,40]. The 1-D WAXD measurement of P4EOPCS/$LiCF_3SO_3$ complex at 200 °C in Fig. 12 shows that the diffraction peak located in the low-angle region of pure P4EOPCS completely disappeared in P4EOPCS/$LiCF_3SO_3$ complex, indicating LC phase formation was disturbed in this case. While in the case of P1EOPCS/$LiCF_3SO_3$ complex samples (Fig. 13), LC order retained when Li^+/[EO] was less than 0.20. The intensity of the diffraction peak in the low-angle region decreased much and the 2θ value in the low-angle region was about 4.6° (d-spacing of 1.9 nm) which is larger than that of P1EOPCS. Further increasing the concentration of Li salt tends to depress the LC phase formation. The temperature-dependent 1-D WAXD measurement of P1EOPCS/$LiCF_3SO_3$ complex (Li^+/[EO] = 0.05) (Fig. 14) shows the LC mesophase developed during heating and retained at high temperatures around 230 °C, as well as on the cooling run, which is quite a typical MJLCP-type LC phase behavior. Therefore, from the 1-D WAXD experiment, Li^+-induced phase transition from Φ_{HN} to Φ_N may appear in MJLCP system, a point that can be strengthened by 2-D WAXD experiments. Different from that of PnEOPCS homopolymers, the 2D-WAXD pattern of Li^+ containing samples exhibited a ring pattern in the low-angle region when the X-ray incident beam was aligned parallel to the film surface (Fig. 15a–c); hexatic diffraction pattern was not observed even with thermal annealing. When the X-ray incident beam was perpendicular to the film surface and parallel to the gradient directions, a pair of diffraction arcs could be seen on the equators, indicating that the ordered structures have developed along the direction perpendicular to the film surface on the

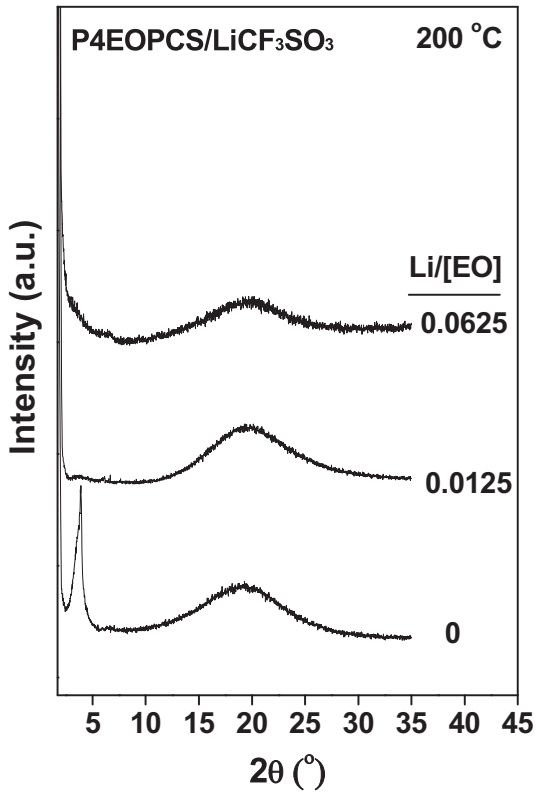

Fig. 12. Set of 1-D WAXD powder patterns for P4EOPCS and corresponding P4EOPCS complex with the lithium salt at 200 °C.

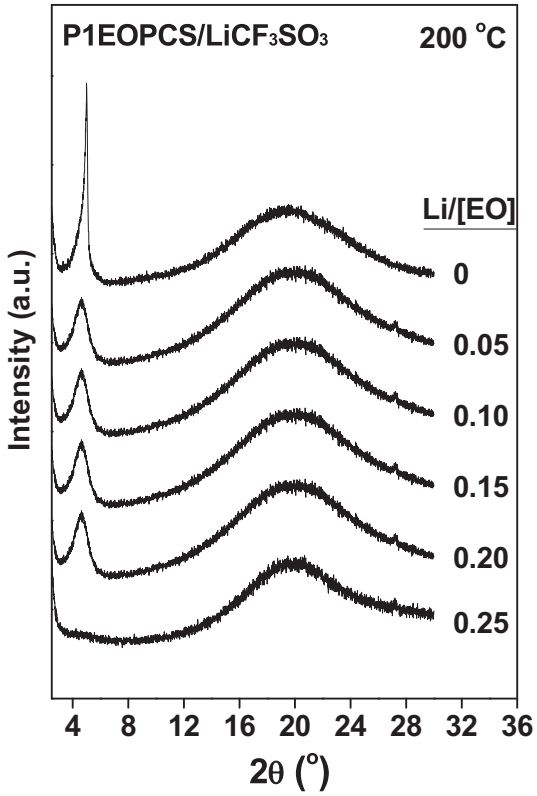

Fig. 13. Set of 1-D WAXD powder patterns for P1EOPCS and corresponding P1EOPCS complex with lithium salts at 200 °C.

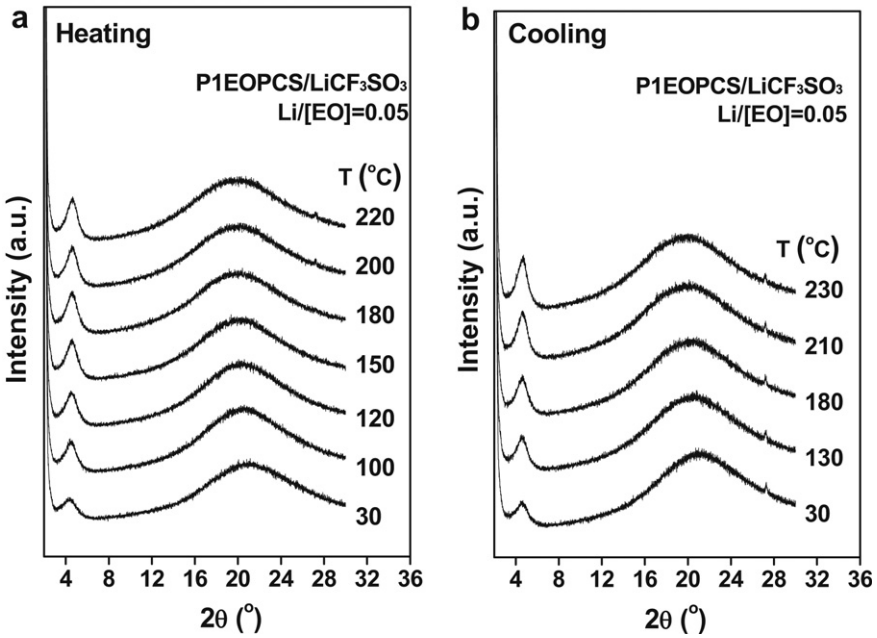

Fig. 14. Set of 1-D WAXD powder pattern of P1EOPCS complex with lithium salts (Li/[EO] = 0.05) obtained during the first heating of the as-cast film (a) and corresponding first cooling WAXD powder pattern of the same film (b).

nanometer scale. Hence, Fig. 15 represents a typical Φ_N diffraction pattern. Note that a very small reflection at $2\theta \sim 27^\circ$ was observed in Figs. 13 and 14 for the Li^+/P1EOPCS complex. The peak seemed to develop upon heating at ~200 °C and remained during cooling. The origin of the peak is not clear at this stage. It is not likely that the peak arose from pure $LiCF_3SO_3$ crystal as other diffraction peaks of $LiCF_3SO_3$ are absent and $2\theta \sim 27^\circ$ is not among the strongest diffraction peaks of $LiCF_3SO_3$. This peak was not observed either in the Li^+/P4EOPCS complex. Further study is needed to clarify this question.

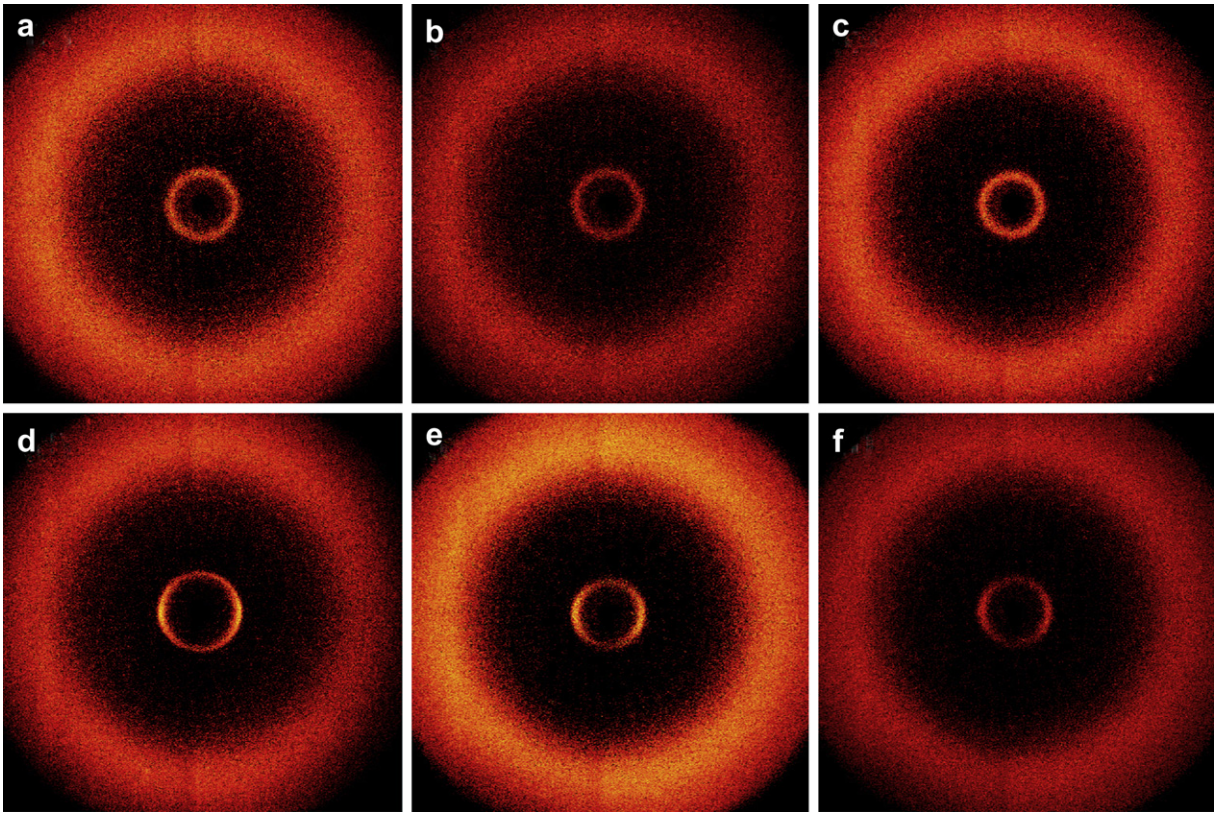

Fig. 15. 2-D WAXD fiber patterns of PnEOPCS (n = 1–3) complex with lithium salt (Li/monomer = 0.1) obtained with the X-ray beam parallel to the shear direction (a: n = 1; b: n = 2; c: n = 3) and perpendicular to the shear direction (d: n = 1; e: n = 2; f: n = 3).

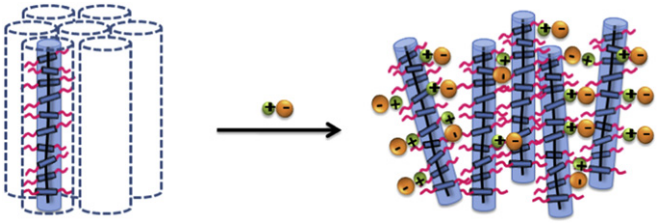

Fig. 16. Schematic representation of the effect of salt complexation on the arrangement of MJLCPs containing oligo(oxyethylene) chains.

Formation of Li^+/[EO] complex in LC systems is known to influence the phase structure of LCs. This is largely due to the dramatic change of EO conformation upon complex formation. In the present system, there are at least two types of physical processes: LC formation driven by the favorable intermesogenic interaction and the Li^+/[EO] complexation [41]. If the desired structures from these two processes prefer similar symmetries and commensurate molecular packing, both processes should be enhanced and we should observe better LC phase order. However, if the desired structures prefer different symmetry and/or molecular packings are incommensurate, the stronger interaction wins and LC symmetry could be distorted had it been the weaker process. This is analogous to the competition between LC phase formation and block copolymer phase separation we recently reported [42]. The aforementioned results show that in the PnEOPCS/$LiCF_3SO_3$, columnar LC phase is incommensurate with Li^+/[EO] complex, hence the longer the EO chains in the LCs, the poorer the resultant LC phase. In P1EOPCS/$LiCF_3SO_3$, hexatic symmetry was broken and Φ_N instead of Φ_{HN} was observed, whereas in P4EOPCS/$LiCF_3SO_3$, even nematic symmetry was broken and the resultant blends did not exhibit LC phase, as shown in Fig. 16. More detailed work is ongoing to reveal the effect of Li^+ on the mesophase behavior of MJLCP systems and the properties of PnEOPCS/$LiCF_3SO_3$ complex.

4. Conclusions

A series of novel MJLCPs, PnEOPCS, have been synthesized using conventional free radical polymerization and ATRP methods. In this system, oligo(oxyethylene) groups were used as the peripheral groups of the lateral mesogens. All the polymers were chemically and mesomorphically thermally stable. Combining 1-D and 2-D WAXD results with PLM and DSC observations, Φ_{HN} and Φ_N phase were identified. These phases arose from the cooperation of the PnEOPCS ($n = 1$–4) backbones and the laterally attached mesogenic groups. X-ray diffraction results showed that the mesogenic side groups were tilted with respect to the backbones. Oligo(oxyethylene) groups rendered a hydrophilicity of the macromolecular rods. The rod surface as well as the LC phases was further tuned by complexation the PnEOPCS with $Li^{\cdot+}$. Columnar LC phase is incommensurate with Li^+/[EO] complex; increasing Li^+ destabilizes LC phases. In P1EOPCS/$LiCF_3SO_3$, LC hexatic symmetry was broken and Φ_N instead of Φ_{HN} was observed, whereas in P4EOPCS/$LiCF_3SO_3$, even nematic symmetry was broken and the resultant blends did not show LC phase.

Acknowledgment

The financial support from the National Natural Science Foundation of China (Grants 20628405 and 20634010) is gratefully acknowledged.

References

[1] Ikkala O, Brinke GT. Science 2002;295(5564):2407–9.
[2] Service RF. Science 2001;293(5531):782–5.
[3] Stupp SI, Braun PV. Science 1997;277(5330):1242–8.
[4] Lehn JM. Science 2002;295(5564):2400–3.
[5] Muthukumar M, Ober CK, Thomas EL. Science 1997;277(5330):1225–32.
[6] Ballauff M. Angew Chem Int Ed Engl 1989;28(3):253–67.
[7] Ungar G. Polymer 1993;34(10):2050–9.
[8] Percec V, Ahn CH, Ungar G, Yeardley DJP, Moller M, Sheiko SS. Nature 1998;391(6663):161–4.
[9] Lee M, Cho BK, Zin WC. Chem Rev 2001;101(12):3869–92.
[10] Ryu JH, Lee M. Liquid crystalline assembly of rod-coil molecules. In: Kato T, editor. Liquid crystalline functional assemblies and their supramolecular structures, vol. 128; 2008. p. 63–98.
[11] Zhou QF, Li HM, Feng XD. Macromolecules 1987;20(1):233–4.
[12] Zhou QF, Li HM, Feng XD. Mol Cryst Liq Cryst 1988;155:73–82.
[13] Zhou QF, Zhu XL, Wen ZQ. Macromolecules 1989;22(1):491–3.
[14] Li CY, Tenneti KK, Zhang D, Zhang HL, Wan XH, Chen EQ, et al. Macromolecules 2004;37(8):2854–60.
[15] Ye C, Zhang HL, Huang Y, Chen EQ, Lu YL, Shen DY, et al. Macromolecules 2004;37(19):7188–96.
[16] Zhi JG, Liu AH, Zhu ZG, Lu XC, Fan XH, Chen XF, et al. Acta Polym Sinica 2005;5:774–8.
[17] Wan XH, Zhang F, Wu PQ, Zhang D, Feng XD, Zhou QF. Macromol Symp 1995;96:207–18.
[18] Chen XF, Tenneti KK, Li CY, Bai YW, Zhou R, Wan XH, et al. Macromolecules 2006;39(2):517–27.
[19] Fabre B, Simonet J. Coord Chem Rev 1998;178:1211–50.
[20] Lauter U, Meyer WH, Wegner G. Macromolecules 1997;30(7):2092–101.
[21] Funahashi M, Shimura H, Yoshio M, Kato T. Functional liquid-crystalline polymers for ionic and electronic conduction. In: Kato T, editor. Liquid crystalline functional assemblies and their supramolecular structures, vol. 128; 2008. p. 151–79.
[22] Yang R, Yang XR, Evans DF, Hendrickson WA, Baker J. J Phys Chem 1990;94(15):6123–5.
[23] Tschierske C. J Mater Chem 1998;8(7):1485–508.
[24] Pugh C, Bae JY, Dharia J, Ge JJ, Cheng SZD. Macromolecules 1998;31(16):5188–200.
[25] Kim GH, Pugh C, Cheng SZD. Macromolecules 2000;33(24):8983–91.
[26] Small AC, Pugh C. Macromolecules 2002;35(6):2105–15.
[27] Arehart SV, Pugh C. J Am Chem Soc 1997;119(13):3027–37.
[28] Gopalan P, Andruzzi L, Li XF, Ober CK. Macromol Chem Phys 2002;203(10–11):1573–83.
[29] Liu YX, Zhang D, Wan XH, Zhou QF. Chin J Polym Sci 1998;16(3):283–8.
[30] Zhang D, Liu YX, Wan XH, Zhou QF. Macromolecules 1999;32(16):5183–5.
[31] He HF, Cao HQ, Wan XH, Tu YF, Chen XF, Zhou QF. Chin Sci Bull 2003;48(14):1485–90.
[32] Sheth JP, Aneja A, Wilkes GL, Yilgor E, Atilla GE, Yilgor I, et al. Polymer 2004;45(20):6919–32.
[33] Yu ZN, Tu HL, Wan XH, Chen XF, Zhou QF. J Polym Sci A Polym Chem 2003;41(10):1454–64.
[34] Zhu ZG, Zhi JG, Liu AH, Cui JX, Tang H, Qiao WQ, et al. J Polym Sci A Polym Chem 2007;45(5):830–47.
[35] Zhao YF, Fan XH, Wan XH, Chen XF, Yi Y, Wang LS, et al. Macromolecules 2006;39(3):948–56.
[36] Chai CP, Zhu XQ, Wang P, Ren MQ, Chen XF, Xu YD, et al. Macromolecules 2007;40(26):9361–70.
[37] Pan QW, Gao LC, Chen XF, Fan XH, Zhou QF. Macromolecules 2007;40(14):4887–94.
[38] Liu AH, Zhi J, Cui JX, Wan XH, Zhou QF. Macromolecules 2007;40(23):8233–43.
[39] Tang H, Zhu ZG, Wan XH, Chen XF, Zhou QF. Macromolecules 2006;39(20):6887–97.
[40] Percec V, Tomazos D. J Mater Chem 1993;3(6):633–42.
[41] Kohmoto S, Mori E, Kishikawa K. J Am Chem Soc 2007;129(44):13364–5.
[42] Tenneti KK, Chen XF, Li CY, Wan XH, Fan XH, Zhou QF, et al. Soft Matter 2008;4(3):458–61.